

# Active Visual Localization in Partially Calibrated Environments

Yingda Yin<sup>1\*</sup> Qingnan Fan<sup>2\*</sup> Fei Xia<sup>2</sup> Qihang Fang<sup>3</sup> Siyan Dong<sup>3</sup>  
 Leonidas Guibas<sup>2</sup> Baoquan Chen<sup>1</sup>

<sup>1</sup>CFCS, Peking University <sup>2</sup>Stanford University <sup>3</sup>Shandong University

{yingda.yin, fqncchina, fqhacad, siyandong.3, baoquan.chen}@gmail.com,

feixia@stanford.edu, guibas@cs.stanford.edu

## Abstract

Humans can robustly localize themselves without a map after they get lost following prominent visual cues or landmarks. In this work, we aim at endowing autonomous agents the same ability. Such ability is important in robotics applications yet very challenging when an agent is exposed to **partially calibrated environments**, where camera images with accurate 6 Degree-of-Freedom pose labels only cover part of the scene. To address the above challenge, we explore using Reinforcement Learning to search for a policy to generate intelligent motions so as to actively localize the agent given visual information in partially calibrated environments. Our core contribution is to formulate the active visual localization problem as a Partially Observable Markov Decision Process and propose an algorithmic framework based on Deep Reinforcement Learning to solve it. We further propose an indoor scene dataset **ACR-6**, which consists of both synthetic and real data and simulates challenging scenarios for active visual localization. We benchmark our algorithm against handcrafted baselines for localization and demonstrate that our approach significantly outperforms them on localization success rate.

## 1. Introduction

The problem of visual localization is defined as estimating the precise 6 Degree-of-Freedom (DoF) camera pose with only visual observations (RGB/RGB-D). This problem plays an important role in many computer vision and robotics applications, *e.g.*, augmented reality [23], visual manipulation, visual navigation [56, 12] and visual mapping [15]. Visual localization faces a number of fundamental yet common challenges, such as repetitive patterns, textureless regions, illumination changes and rearrangement of objects. The popular visual localization approaches [45, 10, 9, 3, 7, 24] are mostly passive, which assume no control of camera movement, and tend to fail under the conditions above. To address these challenges, there has been limited research in the past about active visual localization for mobile robots. The *Active*

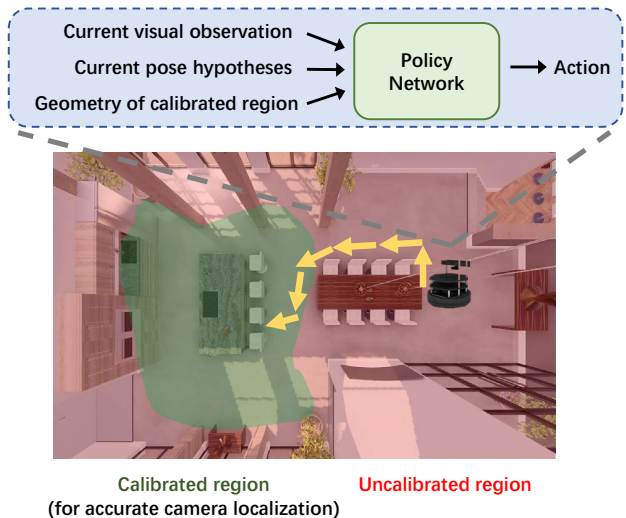


Figure 1: Overview of our problem and approach. We propose to solve the problem of active visual localization in partially calibrated environments. It is formulated as a Partially Observable Markov Decision Process (POMDP), solved within a reinforcement learning framework. The agent decides its movement based on its visual observations, a belief regarding its instant camera pose estimation, and the geometry of the calibrated region.

*Visual Localization* problem is defined as follows: given an initial test frame, active visual localization is to change the camera position and orientation in an active and iterative manner until a new observation is captured that can be used to accurately localize the camera with respect to a known scene.

Early work on active visual localization [14] traces back to the late 1990s, and developed the guiding principle of controlling the robot’s actuators based on the passive Markov localization. There are few following works, all relying on a closed world assumption that the camera is always inside the **calibrated region**, which is visually observed with ground truth camera poses, and can be represented by a grid [11], a topological graph [17] or a visual memory [29]. However, when the camera steps into an **uncalibrated region**, which is not visually observed with ground truth camera poses, as is commonly the case during robot wake-up [13] or navigation

\*Equal Contribution

processes [54], the past passive or active visual localization approaches are both bound to fail due to limited experience learned only from the calibrated scene region.

To make progress on this decades-old problem, we aim for accurate localization in partially calibrated environments, where the precise camera pose is provided for part of the scene – hence the camera will be lost if placed in the uncalibrated region. In order to achieve an efficient and effective solution to this problem, there are two critical questions to ask. 1) “Where to go”: as for a lost camera in the scene, there could exist many available target positions to go for accurate localization. This makes active visual localization intrinsically ambiguous. 2) “When to stop”: as no ground truth camera pose is available during active camera movement, it becomes difficult to determine the stop condition.

In this paper, we propose a novel active visual localization algorithm implemented within a reinforcement learning framework to deal with partially calibrated environments. It consists of two modules, a *camera pose estimator* and a *policy network*. The camera pose estimator learns to map the input visual observation to its corresponding camera pose within the calibrated scene region, which is defined by the provided training sequence of <RGB-D image, camera pose> pairs. The policy learning module formulates the active visual localization problem as a Partially Observable Markov Decision Process (POMDP) [18], implemented as a reinforcement learning algorithm. In each episode, the agent is initialized at a random position in the environment that contains both calibrated and uncalibrated regions, then, to determine “where to go”, the policy learning module guides the agent to navigate towards a novel observation that can be accurately localized with the former pose estimator. As camera pose is not available for supervision, in order to decide “when to stop”, we further design a terminal reward function based on a novel success stop condition triggered by the estimated pose hypotheses.

To validate the effectiveness of our method, we present ACR-6, a new benchmark dataset for training and evaluating the active visual localization algorithms in partially calibrated environments. It consists of 5 high-quality synthetic indoor scenes and 1 scanned real indoor scene, for each of which it provides 1) a training trajectory of <RGB-D image, camera pose> pair that partially covers the scene, 2) the full textured 3D scene mesh, 3) dynamic scenes with geometric and illumination changes, and 4) validation and test image set. Experimental results on the ACR-6 dataset demonstrate that our proposed algorithm outperforms the state-of-the-art (passive) localization approaches by 568% in localization success rate, and surpasses our best performing handcrafted active visual localization baselines by 91% in localization success rate.

Our contributions in this work can be summarized as follows,

- We propose a novel active visual localization algorithm to deal with partially calibrated environments. Our al-

gorithm is formulated as a Partially Observable Markov Decision Process (POMDP) solved within a reinforcement learning framework.

- We present ACR-6, a new benchmark dataset for training and evaluation of the active visual localization problem. It includes 6 high-quality indoor scenes, equipped with training sequence, 3D scene mesh, dynamic scenes, validation and test image set.
- Our proposed algorithm outperforms the existing localization approaches by a large margin and surpasses the designed active visual localization baselines with much higher accuracy.

## 2. Related Work

**Visual localization.** The task of visual localization is to estimate a 6 DoF camera pose from visual observation. The early work explored various image features to retrieve the most similar database image for pose approximation of a reference image. The traditional retrieval-based approaches mostly rely on hand-crafted features [39, 25, 38, 40], such as SIFT [27], which are replaced with the recent deep learning features [1, 37, 36, 48]. Besides image retrieval, a different popular trend for visual localization is to learn a deep neural network that directly maps a reference image to its corresponding camera pose. The pioneer work in this direction is known as PoseNet [20] with many followups [19, 52, 8]. However, the recent work [42] observe that the learning-based direct pose estimation approaches perform similarly to the type of image retrieval methods.

The aforementioned approaches run in an end-to-end manner for direct pose estimation. The other type of literature employs a two-step procedure, where the first step is to regress the 3D scene coordinate from the input RGB/RGB-D observation, and the second step takes a RANSAC based optimization to produce the final camera pose according to the 2D/3D-3D correspondence constructed from the first step. The popular scene coordinate regression approaches are implemented as a regression forest [45, 30, 32, 33, 16, 4, 50, 10, 9] or a convolution neural network [3, 5, 7, 6, 55, 24]. These approaches builds structure-based knowledge in a more explicit way, and performs better than image retrieval on small- or middle- scale environments.

The aforementioned approaches are all passive and vulnerable to a number of challenges, such as dynamic environments and highly ambiguous regions. There emerge a few works [14, 11, 17, 29] regarding active localization to resolve the above issues. However, these approaches mainly leverage the past visual experience to construct a grid [14, 11], topological graph [17, 12] or visual memory [29] as guidance for active localization, which significantly boosts the localization performance, while on the other hand limits their algorithm to be robust in uncalibrated scene regions. In this paper, we target active visual localization in partially calibrated environments, which has not been discussed much

in the past and the existing works can not be applied to our scenario.

**Reinforcement learning for active vision.** Reinforcement learning has boosted the state of the art of many computer vision tasks, *e.g.*, object detection [31], tracking [35, 47], 3D shape modelling [26], and 3D part discovery [28]. A few recent works focus on the 3D pose estimation and refinement of objects. [22] optimizes the parameters of an existing state-of-the-art object pose estimation system via learning to select the optimal pose hypotheses within a limited computational budget. [44] proposes a pose-free reinforcement learning approach to refine the 6D pose by learning to manipulate the 3D model. [46] tackles the problem of accurate object pose estimation through camera movement towards the uncertain objects.

Unlike the aforementioned approaches that mostly focus on the object space, in this work, we aim at camera pose estimation with respect to a scene-level environment without the ground truth pose supervision for policy learning.

**3D scene dataset for visual localization.** The scene level datasets developed for visual localization can mostly be categorized into outdoor and indoor datasets. The outdoor ones [2, 41] usually characterize day-night, season and weather changes, or middle-/large-scale geometric changes, *e.g.*, cars and buildings. However, the 3D scene models in these datasets are either missing or constructed in the format of sparse point cloud, which is not suitable to render high-quality visual observations at any unpredictable position for reinforcement learning. On the other side, the indoor datasets in the past cover both room-level environments [45, 49, 51] and large-scale university buildings [48]. The constructed training and test scene meshes in these scanned real datasets mostly do not fully overlap with each other, and sometimes lack important geometric details, such as walls, which are however required to obtain a complete full-frame visual observation for real-time rendering in reinforcement learning.

As a benefited of the highly-controlled synthetic environments, our proposed ACR-6 dataset provides high-quality 3D scene mesh during both training and test. We also scan a real indoor scene covering bedroom, living room and kitchen to demonstrate the robustness of our algorithm on real-world environments.

### 3. Problem Definition

Provided a sequence of <RGB-D image, camera pose> pairs, denoted as  $\{I_i^{\text{train}}, C_i^{\text{train}}\}_{i=1}^m$  where  $m$  is the number of images, that covers the partial scene where camera is calibrated, and an initial test frame  $I_0$  sampled in the entire scene, the task of active visual localization is to translate and rotate the camera in an active manner until reaching a new frame  $I_t$  where an accurate camera pose  $C_t$  can be estimated. This problem can be naturally formulated into a Partial Observable Markov Decision Process (POMDP)

defined by the tuple  $\mathcal{M} = (\mathcal{S}, \mathcal{A}, \mathcal{O}, \mathcal{T}, \mathcal{R})$ . Here,  $\mathcal{S}$  is the state space;  $\mathcal{A}$  is the action space;  $\mathcal{O}$  is the observation space;  $\mathcal{T}(s'|s, a)$  is the state transition function,  $s \in \mathcal{S}$ ,  $a \in \mathcal{A}$  and  $s'$  is the new state;  $\mathcal{R}(s, a)$  is the reward function.

We assume that the state is not directly observable and learn a policy  $\pi(a|o)$  conditioned on observations  $o \in \mathcal{O}$  to generate the action  $a$ . Its goal is to maximize the expected discounted reward  $\mathbb{E}_{a \sim \pi}[\sum_{t \geq 0} \gamma^t r_t]$ , where  $\gamma \in [0, 1)$  is the discount factor, and  $r_t$  is the immediate reward at time step  $t$ . As a deviation from the classic POMDP setup, our real reward is not directly observable due to the unavailability of ground truth camera pose for policy learning, which makes the problem even more challenging. In the next section, we provide the instantiation of each space and how we formulate a surrogate reward.

## 4. Approach

In order to solve this problem, in this paper, we propose a novel active visual localization algorithm. Its full pipeline is illustrated in Figure 2(a), and can be separated into two steps, 1) building a camera pose estimator and 2) a reinforcement learning (RL) framework for localization, which are detailed below.

### 4.1. Camera Pose Estimator

The input consecutive image observations along with their corresponding ground truth camera poses provide the basic 3D knowledge of the partial calibrated indoor scene. To take advantage of the fact that it is possible for the agent to localize accurately when observing the calibrated region, we build a camera pose estimator, denoted as  $E$ , using the above sequence to project the input image  $I_i^{\text{train}}$  to its camera pose  $C_i^{\text{train}}$ . We employ the state-of-the-art structure-based camera relocation algorithm, regression forest [10], as our pose estimator. The pose estimator serves only as a tool to facilitate the following RL framework, and our solution is general in the sense that this module is replaceable with other visual localization solutions.

### 4.2. Reinforcement Learning for Localization

Given the pretrained camera pose estimator, the goal of the reinforcement learning algorithm is to progressively move the agent from an initial bad observation to a new observation that can be accurately localized. The camera pose estimator is used as-is and no longer finetuned in this stage due to the lack of ground truth camera pose. Moreover, the pose estimator is trained solely on the provided consecutive images, which may not fully cover the whole indoor scene, while the agent has the full access to the same scene when training reinforcement learning algorithm. The state space, observation space, action space and reward function of the RL algorithm are detailed below.

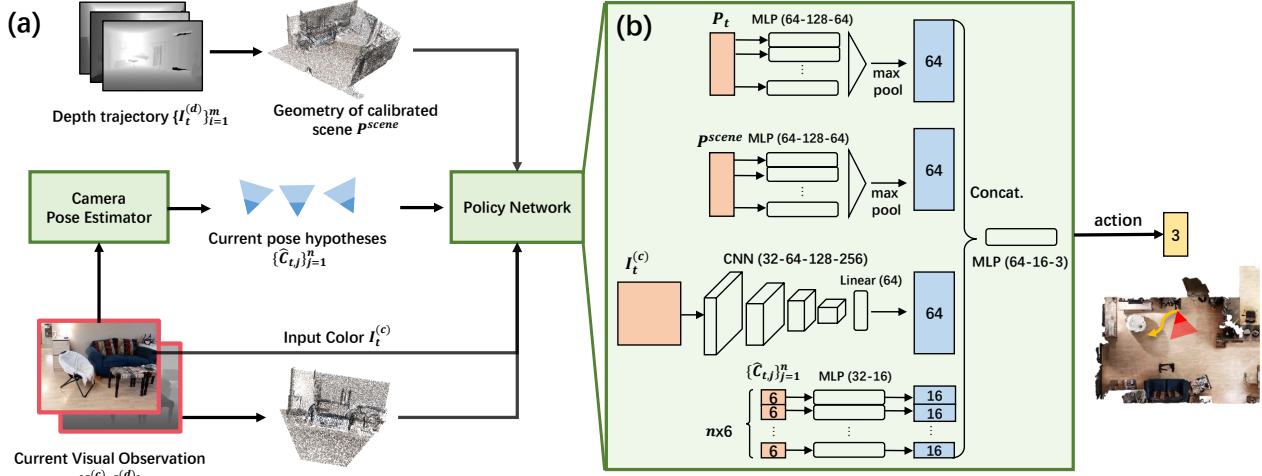


Figure 2: (a) The proposed active visual localization algorithm. The entire pipeline takes two steps: 1) it builds a camera pose estimator using the given sequence of <RGB-D image, camera pose> pair; 2) having the agent randomly positioned and oriented in the calibrated scene, it learns a policy network that takes the current visual observation, pose hypotheses, and geometry of calibrated region as input, in order to learn intelligent actions to obtain a new observation that can be accurately localized. (b) Architecture of the policy network.

#### 4.2.1 State Space

The state space of the agent indicates the ground truth of agent’s position and orientation with respect to the map frame. Specifically, the state at time step  $t$  is represented as a 3D tensor,  $s_t = (x_t, y_t, \theta_t)$ , where  $x_t, y_t$  are the agent locations within the 2D scene map, and  $\theta_t$  is the agent orientation that ranges from  $0^\circ$  to  $360^\circ$ . These values not visible to the agent while the agent keeps track of the observation  $o_t$  for policy learning.

#### 4.2.2 Observation Space

The observation design should encode the knowledge of the current sensor input and the scene, and have positive guidance for the agents to move towards the position acknowledged by the pretrained camera pose estimator. In order to achieve this goal, we define the observation at time step  $t$  as the combination of the following four components:  $o_t = \{I_t^{(c)}, \{\hat{C}_{t,j}\}_{j=1}^n, P_t, P^{scene}\}$ , where  $n$  is a hyperparameter denoting how many pose hypotheses to use.

**Current visual observation.** The most direct signal given to the agent is the current visual input  $I_t = \{I_t^{(c)}, I_t^{(d)}\}$ , which is the simulated sensor output from the agent’s current accurate pose. The visual observation consists of both RGB color  $I_t^{(c)}$  and depth  $I_t^{(d)}$ . The 2D depth is further lifted to the 3D camera coordinates  $P_t$  with the camera intrinsics for policy learning.

**Current pose hypotheses.** The camera pose estimator takes the RGB-D frame as input and generates a number of pose hypotheses  $\{\hat{C}_{t,j}\}_{j=1}^n = E(I_t)$  after employing the preemptive, locally-optimized RANSAC. We rank the pose hypotheses according to the computed scores in [10], in

order to select the best  $n$  hypotheses, which demonstrate the most confident camera pose estimations for the current observation and hence serve for the policy update.

**Geometry of calibrated region.** Accurate camera pose can be computed with correct 3D-3D point correspondence established between the geometry of current observation in camera space  $P_t$  and calibrated scene region in world space  $P^{scene}$ , which in turn should benefit learning navigation behavior. We define a 3D point in the scene geometry to be calibrated as it is observed by a visual input with ground truth camera pose. Hence, we compute  $P^{scene}$  by firstly projecting the depth images in the training sequence into world coordinates using the ground truth camera poses, and then fusing all the world coordinates into the point cloud of the calibrated scene region.

#### 4.2.3 Action Space and State Transition

The agent is capable of performing three actions, *move forward*, *turn left* and *turn right*. At each time step, the agent will choose one action among the three to obtain a new observation.  $\mathcal{A} = \{\text{left, right, forward}\}$ .

To simulate robotic agents in a real world condition, the action does not lead to perfect execution, hence we add noise on the actions with the state transition function  $\mathcal{T}$ , which is defined as:

$$s'_t - s_t \sim \begin{cases} \mathcal{N}(\mu_l, \Sigma_l), & \text{if } a_t = \text{left}, \\ \mathcal{N}(\mu_r, \Sigma_r), & \text{if } a_t = \text{right}, \\ \mathcal{N}(\mu_f, \Sigma_f), & \text{if } a_t = \text{forward}. \end{cases} \quad (1)$$

where  $a_t$  is the sampled action,  $\mathcal{N}$ ,  $\mu$ ,  $\Sigma$  are the Gaussian distribution along with its mean and covariance matrix. The

subscript  $l, r, f$  refers to the action of *turn left*, *turn right* and *move forward*.

The design of action space is decided by the target embodiment, which we choose to be a robot in this paper, as it can be directly applied to facilitate the localization step in the visual navigation task. The action space can also be further extended to be more complex, such as 6 DoF if required, which however is not the focus of this work.

#### 4.2.4 Reward Estimation

At each time step, the agent will receive a reward and later use it to update the policy network. In the classical POMDP setup, the reward  $\mathcal{R}(s, a)$  is a function of state and action pair. However in our case, the state is not visible to the agent, and the real reward is also unavailable due to the lack of ground truth camera pose. Hence we design a surrogate reward  $\hat{\mathcal{R}}(o, a)$  defined on the observation and action. The total reward consists of the slack reward  $\hat{\mathcal{R}}_{slack}$  and terminal reward  $\hat{\mathcal{R}}_{stop}$ , which are detailed below.

**Terminal reward** is to either punish the failure stop or award the success stop. The failure stop happens when the agent reaches the predefined maximum allowed time steps, collides with any object, or the camera pose estimator returns NULL due to systematic error. The success stop is non-trivial to determine in the active visual localization problem since the agent is not aware of the ground truth camera pose except for the provided image observations, and this makes our problem highly ambiguous and dramatically different from the others, such as robotic navigation or manipulation tasks, which mostly have a deterministic goal. In order to decide when the agent successfully reaches an accurate camera pose with high confidence, we calculate the variance  $v_t$  of the four pose hypotheses and define the variance threshold  $v_{thres}$ , we consider a success stop when  $v_t \leq v_{thres}$ . In the later experimental session, we observe that the success stop judgements usually conform to highly accurate camera pose estimations, which phenomenon justifies the effectiveness of the proposed *hypotheses variance*  $v_t$ . Then the terminal reward is defined as,

$$\hat{\mathcal{R}}_{stop} = \begin{cases} 100, & \text{if success: } v_t \leq v_{thres}, \\ -100, & \text{if failure (out of bound, timeout)} \end{cases} \quad (2)$$

**Slack reward** is used to punish unnecessary steps and keep the path efficient. Let  $\tau$  denotes the total time steps that the agent takes until meeting the stop criterion in one episode, and the punishment for each time step is empirically set as 5, then the slack reward is defined as,

$$\hat{\mathcal{R}}_{slack} = -5\tau \quad (3)$$

The final reward is the weighted summation of both the aforementioned rewards in each navigation episode,

$$\hat{\mathcal{R}} = \hat{\mathcal{R}}_{slack} + \lambda \hat{\mathcal{R}}_{stop} \quad (4)$$

where  $\lambda$  is the hyper parameter to balance the weights between the two reward terms. Please refer to Sec 6.1 and the Supplementary Material for information about hyper parameters described in this section.

#### 4.2.5 Policy Network

The policy network takes the observation  $o_t$  as input and generates the probability of the three actions defined by the action space  $\mathcal{A}$ . Its structure is illustrated in Figure 2(b). The input geometry of current observation  $P_t$  and calibrated scene region  $P^{scene}$  are both represented as 3D coordinates, the same as point cloud. Inspired by the popular point cloud processing network PointNet [34], for both  $P_t$  and  $P^{scene}$ , we employ a three-layer pointwise MLP (64-128-64) followed by a max pooling layer to extract its global feature ( $\mathbb{R}^{64}$ ).  $P_t$  and  $P^{scene}$  shares the same network architecture yet with different learned weights. For the input frame  $I_t$ , we employ a convolution neural network of 4 convolution layers (32-64-128-256) and 1 linear layer (64) to extract the global feature ( $\mathbb{R}^{64}$ ). Each convolution layer is of kernel size 3x3 and followed by a batch normalization layer and a max pooling layer of stride 2. Each input pose hypothesis  $\hat{C}_{t,j}$  is represented as a 6D tensor that consists of 3D translation and 3D rotation (Euler angles), and we leverage a two-layer MLP (32-16) to extract its feature ( $\mathbb{R}^{16}$ ). Finally, by concatenating all the extracted features, we use a three-layer MLP (64-16-3) to predict the probability of the three predefined actions.

## 5. ACR-6 Dataset

As discussed in Sec. 2, we need a dataset that supports changing layout, photorealistic rendering and real time rendering to benchmark our algorithm on active visual localization problem. So we propose a new benchmark dataset, namely ACR-6 dataset, to facilitate the training and evaluation for the active visual localization problem. We are committed to release this dataset to the research community. In order to construct such a dataset, we collect 5 high-quality synthetic indoor scenes, which are created by professional interior designers, and hence feature realistic texture, lighting, layout and high resolution mesh. We also scanned one real indoor scene to further test the robustness of our algorithm in real-world environments. For each scene, we also provide a “dynamic” counterpart to it, we denote them as  $s_{x-d}$  and  $r_{0-d}$ . The “dynamic” scene is a perturbed version of the original scene, in furniture arrangements as well as lighting. For the difference between original scene and dynamic scene, please refer to the Supplementary Material.

For each indoor scene, we provide a list of data as follows:

- A training trajectory of  $\langle \text{RGB-D image, camera pose} \rangle$  pairs that observes the partial scene where the camera is calibrated.
- The full 3D scene mesh and its photorealistic texture that includes both calibrated and uncalibrated regions.

- The dynamic scene (textured mesh) that characterizes the illumination and geometric changes to test the robustness of the visual localization algorithms.
- The validation and test split for benchmarking purposes. Each split consists of 1000 initial positions randomly sampled from the entire scene, and are provided for both the original static and modified dynamic scenes.

The full 3D scene meshes are shown in Fig. 3, and the related statistics are demonstrated in Table 1.

For purpose of reinforcement learning, the ACR-6 dataset supports real-time photorealistic rendering from high-quality scene meshes. For the synthetic indoor scene, real-time rendering usually sacrifices the rendering quality. To tackle this challenge, we take advantage of the texture baking workflow. It firstly employs a physically-based renderer to generate the photorealistic images that cover the whole indoor scene, and then optimizes the mesh and texture using the above high-quality rendered images, finally real-time photorealistic rendering can be achieved using the optimized scene without losing much image quality. In the implementation, we employ Cycles to render the photorealistic images, and the real-time renderer in Interactive Gibson [53] to synthesize camera images for reinforcement learning. For the real indoor scene, the texture is realistic in nature, but the constructed scene meshes tend to have some artifacts due to the limited scanner in the existing visual localization datasets [45, 49, 51]. We take advantage of the Matterport scanner device along with its scene reconstruction algorithms to obtain the high-quality complete indoor scene mesh, and achieve real-time rendering also in Interactive Gibson.

## 6. Experiments

### 6.1. Implementation Details

In our experiment, we use the state-of-the-art off-policy learning method Proximal Policy Optimization (PPO) [43] as the policy optimizer. We employ the Adam [21] to optimize the network weights with initial learning rate  $3 \times 10^{-4}$ . Some hyper-parameters:  $v_{thres} = 10^{-4}$ ;  $\lambda = 2$ ;  $\gamma = 0.99$ .

The state  $s_t = (x_t, y_t, \theta_t)$  is perturbed with Gaussian noise to generate the new state  $s'_t$  according to the chosen action as shown in the state transition function. To be specific, if the agent turns left or right, the Gaussian noise of mean (30/-30) and standard deviation (6) will be added on the rotation angle  $\theta_t$ ; if the agent moves forward, the Gaussian noise of mean (20) and standard deviation (5) will be added on the 2D positions  $x_t, y_t$ . The positions are measured in centimeters, and the rotation angle is measured in degrees.

### 6.2. Baselines

Since the most related work on active visual localization [11] requires a full map and is not specifically designed for partially calibrated scenes, we cannot directly compare with their algorithm. Therefore, we propose several baseline approaches for comparison. **No-movement** indicates the

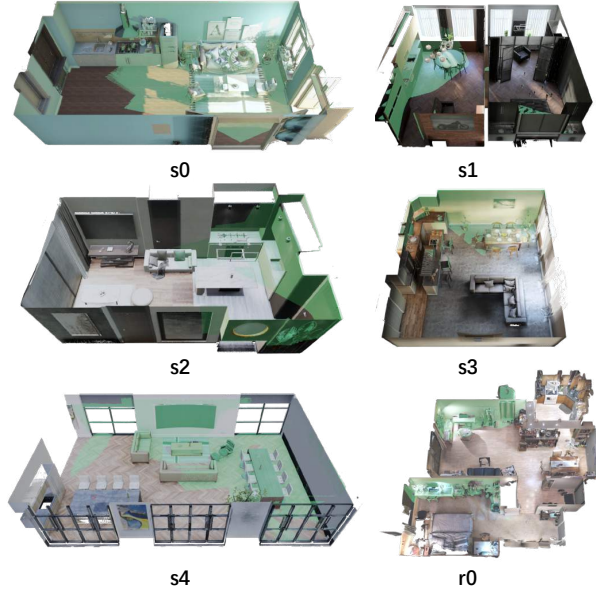


Figure 3: Scenes in ACR-6 datasets, where  $s_0$ - $s_4$  are synthetic scene and  $r_0$  is the scanned real scene. Zoom in to see the details. The green shaded area indicates calibrated regions.

Scene	Area ( $m^2$ )	#training frames	calibrated regions
$s_0$	34.4	700	38.4%
$s_1$	40.0	120	22.2%
$s_2$	19.7	100	20.2%
$s_3$	36.5	80	20.8%
$s_4$	103.0	310	35.3%
$r_0$	56.3	260	12.0%

Table 1: Scene statistics of ACR-6 dataset.

visual localization result of the initial test frame predicted by the pretrained camera pose estimator. This baseline is used to demonstrate how inaccurate the initialization is, and how much improvement the other approaches can achieve. **Turn-around** means the agent turns a circle along the vertical z axis without any forward movement, and stops at the estimated case pose with lowest hypotheses variance  $v^{(t)}$ . It simulates a common localization strategy in real-life visual navigation solutions. At each time step, **Random action** chooses a random action, and **Greedy action** tries all the actions once and selects the one with the lowest hypotheses variance  $v^{(t)}$ . Both of these two strategies enable agent navigation, and stop when triggering the success/failure condition same as our algorithm.

### 6.3. Evaluation Metrics

The performance of active visual localization is evaluated on **accuracy**. It employs the camera pose accuracy computed as the proportion of successful test frames whose

Scene	s0	s1	s2	s3	s4	r0	Avg.
No-movement	(0.155, 0)	(0.180, 0)	(0.149, 0)	(0.180, 0)	(0.105, 0)	(0.136, 0)	(0.151, 0)
Turn-around	(0.488, 15.2)	(0.459, 15.1)	(0.510, 15.0)	(0.589, 15.2)	(0.424, 15.2)	(0.486, 15.1)	(0.493, 15.1)
Random	(0.299, 20.8)	(0.330, 11.3)	(0.162, 14.7)	(0.292, 12.9)	(0.229, 28.0)	(0.207, 12.2)	(0.253, 16.7)
Greedy	(0.484, 15.2)	(0.380, 5.0)	(0.312, 11.4)	(0.358, 7.4)	(0.325, 14.4)	(0.297, 8.4)	(0.359, 10.3)
Ours	<b>(0.966, 14.0)</b>	<b>(0.896, 12.3)</b>	<b>(0.876, 12.7)</b>	<b>(0.913, 8.6)</b>	<b>(0.870, 15.2)</b>	<b>(0.958, 15.6)</b>	<b>(0.913, 13.1)</b>

Scene	s0-d	s1-d	s2-d	s3-d	s4-d	r0-d	Avg.
No-movement	(0.132, 0)	(0.118, 0)	(0.110, 0)	(0.083, 0)	(0.056, 0)	(0.095, 0)	(0.099, 0)
Turn-around	(0.447, 15.3)	(0.403, 15.3)	(0.385, 15.2)	(0.345, 15.0)	(0.287, 15.2)	(0.392, 15.2)	(0.377, 15.2)
Random	(0.223, 20.3)	(0.225, 13.7)	(0.063, 14.0)	(0.200, 11.7)	(0.100, 37.1)	(0.153, 17.6)	(0.161, 19.0)
Greedy	(0.336, 14.8)	(0.297, 7.0)	(0.174, 14.0)	(0.270, 8.3)	(0.199, 26.4)	(0.213, 12.1)	(0.248, 13.8)
Ours	<b>(0.886, 19.7)</b>	<b>(0.773, 14.7)</b>	<b>(0.760, 26.8)</b>	<b>(0.837, 11.6)</b>	<b>(0.700, 42.3)</b>	<b>(0.711, 20.9)</b>	<b>(0.778, 22.7)</b>

Table 2: Active camera localization performance compared with baselines on the ACR-6 dataset. The metrics are formulated as (accuracy, #steps).  $s_x-d$  denotes the dynamic variant of  $s_x$ .

	Static	Dynamic
w/o geometry & color	(0.742, 18.0)	(0.738, 20.4)
w/o geometry	(0.890, 11.1)	(0.749, 11.2)
Ours	<b>(0.896, 12.4)</b>	<b>(0.773, 14.7)</b>

Table 3: Analysis of input modalities. The metrics are formulated as (accuracy, #steps).

translation error is within 5cm and rotation error is within  $5^\circ$ , while only the last test frame in an episode where the robot reaches the stop condition is considered into calculating the accuracy. The success stop condition is only judged by the predicted pose hypotheses, and it indicates how confident the agent “believes” it succeeds in localization which may actually fail. In order to evaluate how consistent the “believed” success stop cases are to the real success stop cases defined by the accuracy measure, we propose **successIOU**, which is computed as the intersection between the above two success stop cases over the union of them. Notice successIOU is only to measure the effectiveness of our designed success stop condition, not for comparison among different approaches.

We further compute **#steps**, which is the average number of steps for all the successful navigation episodes acknowledged by the accuracy measure. It is only a complementary metric to evaluate the efficiency of the path, while we value the accuracy most.

## 6.4. Results

**Quantitative results.** The quantitative results in ACR-6 test set are shown in Table. 2. The No-movement baseline achieves only an average of 15.1% accuracy in static scenes and 9.9% accuracy in their dynamic variants, suggesting moving the agent is crucial for successful visual localization in partially calibrated environments. The Turn-Around heuristic is about to achieve 49.3% in static scenes and 37.7% accuracy in their dynamic variants, suggesting turning around is a simple yet effective heuristic, which is the reason it is commonly used in many robotics appli-

Parameter	Value	Static	Dynamic
$v_{thres}$	$2 \times 10^{-5}$	(0.842, 14.3, 0.998)	(0.770, 20.6, 0.997)
	$5 \times 10^{-5}$	(0.880, 12.7, 0.991)	(0.771, 14.3, 0.996)
	$1 \times 10^{-4}$	<b>(0.896, 12.3, 0.979)</b>	(0.773, 14.7, 0.983)
	$2 \times 10^{-4}$	(0.858, 10.7, 0.974)	<b>(0.775, 13.3, 0.958)</b>
	$5 \times 10^{-4}$	(0.780, 8.7, 0.863)	(0.761, 11.5, 0.941)
$n$	2	(0.408, 3.863, 0.426)	(0.286, 5.269, 0.302)
	4	(0.896, 12.3, 0.979)	<b>(0.773, 14.7, 0.983)</b>
	6	<b>(0.901, 14.0, 0.998)</b>	(0.734, 15.345, 0.999)

Table 4: Analysis of the variance convergence threshold and number of pose hypotheses. The metrics are in (accuracy, #steps, successIOU).

cations. Greedy and Random in general performs worse than Turn-around, but the number of steps used might be smaller, because these two methods are more flexible than Turn-around.

Our approach achieves an average of 90.6% accuracy in static scenes and 78.8% accuracy in their corresponding dynamic variants. It outperforms the passive localization baseline (No-movement) by 568%, and the other active localization baselines by at least 91%, thanks to the intelligent behaviour learned by our proposed reinforcement learning based framework. This result stands in both static scene and dynamic scenes. However, dynamic scenes create further challenges apart from uncalibrated regions, hence the performance here is in general lower than the one in static scenes.

**Qualitative results.** We visualized the trajectory of our method in Fig. 4. Upon inspection, the learned policy exhibits many intelligent behaviors emerges from RL training. For example, it can trace a long path from an uncalibrated region to calibrated region (a)(b), and turn-around in place when facing away calibrated region (d). When trained in a static environment and tested in a dynamic environment, it will try to find the familiar regions (c). It also learns to avoid texture-less regions and actively resolve symmetry (e)(f).

## 6.5. Ablation Study and Analysis

For sake of simplicity, the experiments in this section are all conducted on a representative scene  $s_1$  of the ACR-6 dataset.

**Input modalities.** Our policy network consumes the geometry of calibrated scene and current observation  $\{P_t, P_{scene}\}$ , current observed color information  $\{I_t^{(c)}\}$  and pose hypotheses  $\{\hat{C}_{t,j}\}_{j=1}^n$ . We gather the evidence that each modality is useful by running 3 experiments with different input modalities: All modalities, without geometry, and without both geometry and color. For the variant with reduced modalities, the corresponding feature encoding branches in the policy network is removed. The results are shown in Table 3. The performance degrades as we gradually remove modalities. This is expected and demonstrates that both geometry and color information do help. It also provides evidence that the agent is able to use context information to plan more effective paths towards localizable regions.

**Analysis of variance threshold  $v_{thres}$ .** The success of our algorithm critically depends on the design of the success stop condition, which is determined by the variance threshold  $v_{thres}$ . Therefore, in this experiment, we test the effect  $v_{thres}$  has on our algorithm. We test 5 different values from low to high in Table 4, and observe that as  $v_{thres}$  increases, the successIOU and #steps gradually degrades. This demonstrates that our proposed success stop condition triggered by the camera pose hypotheses is very effective with a small variance threshold, which however may make the reinforcement learning framework difficult to achieve real success as the localizable regions will also be smaller controlled by  $v_{thres}$ . This is verified by the experiment that the best accuracy is actually achieved by an intermediate  $v_{thres}$ , not the smallest one.

**Analysis of number of hypotheses  $n$ .** The performance of using different numbers of pose hypothesis is shown in Table 4. Using  $n = 2$  causing an inaccurate (often optimistic) estimation of pose variance, causing performance to degrade. Using  $n = 6$  results in better pose variance estimation at the cost of additional computation. Empirically, using  $n = 6$  also causes performance to drop in dynamic scenes, so we used  $n = 4$  in our main experiments.

**Robustness to camera pose estimator.** We swap the camera pose estimator to DSAC++ [5] and test the performance. The performance of using DSAC++ as camera pose estimator yields a success rate of 0.888 in static scenes, which is comparable to using regression forest [10] as camera pose estimator (0.896), indicating that our framework is agnostic to the camera pose estimator used.

**Running time.** The averaged time for each step of our algorithm during inference is 224ms on an Nvidia GTX 2080Ti GPU, indicating that our approach can be used a real robots that require real-time predictions of actions.

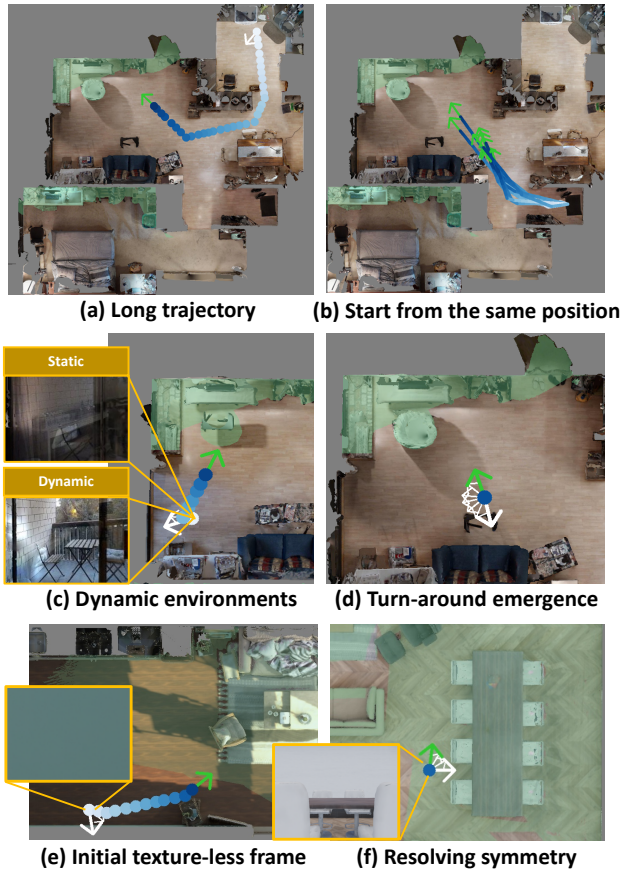


Figure 4: Qualitative Results. The agent learns various intelligent behaviors for active visual localization. White arrow: start position; Green arrow: end position (successfully localized); Light green region: calibrated region for accurate localization; Static/Dynamic: different captured frames in static and dynamic environments. The dots with color gradient indicate the path the agent takes. (a) The agent is able to travel along a long trajectory from an uncalibrated area to a calibrated area. (b) Starting from the same location, the agent generally travels to the same target region. (c) Even placed in the dynamic environment, the agent can still actively localize itself by exploring and finding a familiar region. (d) Emergence of turn around behavior. (e) The agent is able to turn around upon seeing texture-less region. (f) The agent actively turns around when the initial frame results in ambiguity in localization. Zoom in to see the details.

## 7. Conclusion and Future Work

In this paper, we propose an algorithm to solve the active visual localization problem in partially calibrated environments. We formulate this problem as a Partially Observable Markov Decision Process (POMDP) and solved with a reinforcement learning framework. Our approach is evaluated in our proposed dataset, namely ACR-6, containing challenging relocalization cases in partially calibrated and dynamic environments. Our algorithm outperforms the compared approaches on camera pose accuracy by a significant margin. In the future, we would like to extend our framework to

be able to update the camera pose estimator along with RL training, so that the agent can learn to localize in a life-long learning setting. We would also validate the algorithm on a robot platform in the real world.

## 8. Appendix

The appendix provides the additional supplemental material that cannot be included into the main paper due to its page limit:

- Camera Pose Estimation for Active Localization.
- Generalization to Novel Scenes.
- Performance in Both Localizable and Unlocalizable Regions.
- Training Curves.
- More Details of the ACR-6 Dataset.
- More Visual Results.

### A. Camera Pose Estimation for Active Localization

Once the reinforcement learning algorithm finishes one episode triggered by the success or failure stop condition, the **final** camera pose will be selected from the generated pose hypotheses by iterative refinement following [5, 10].

### B. Generalization to Novel Scenes

In order to move the agent from an initial bad observation to a new localizable observation in the partially calibrated environments, the policy network learns scene-specific prior for active guidance. To test its generalization capability to novel scenes that the policy network does not observe during training, we conduct two experiments, 1) train the policy network on  $s_0$  and test on  $s_1$ ; 2) train the policy network on  $s_1$  and test on  $s_0$ .

The numerical results are shown in Table 5. We observe that the generalization version achieves much worse performance compared to our original version, yet is still comparable to the baselines. Especially when the policy network is trained on  $s_0$  and tested on  $s_1$ , the accuracy is surprisingly much better than all the baselines. It demonstrates the promising generalization ability of our algorithm on novel scenes, which however is not the focus of this work and can be explored deeper in the future work.

### C. Performance in Both Localizable and Unlocalizable Regions

To study our learned behavior on the easy and difficult cases individually, we separate the indoor scene into localizable and unlocalizable region. The localizable region is defined as the area where the simple “Turn-around” baseline succeeds, hence theoretically the agent can naively learn the rotation actions only. The unlocalizable region is all

Scene	$s_0$	$s_1$
No-movement	(0.155, 0)	(0.180, 0)
Turn-around	(0.488, 15.2)	(0.459, 15.1)
Random	(0.299, 20.8)	(0.330, 11.3)
Greedy	(0.484, 15.2)	(0.380, 5.0)
Ours (generalize)	(0.478, 26.2)	(0.600, 22.6)
Ours	<b>(0.966, 14.0)</b>	<b>(0.896, 12.3)</b>

Table 5: Generalization to novel scenes. The metrics are formulated as (accuracy, #steps). “Ours (generalize)” denotes the version trained on  $s_0$  and test on  $s_1$ , or trained on  $s_1$  and test on  $s_0$ .

the other areas in the environment where the agent needs to at least move forward in order to find a better position for accurate localization.

Based on the above definition, we separate the test images in ACR-6 dataset into localizable and unlocalizable ones, and calculate their performance in Table 6. As expected, within the localizable region, our algorithm is able to succeed in much fewer steps, and achieves higher accuracy, while within the unlocalizable region, our algorithm takes longer steps and achieves lower accuracy.

### D. Training Curves

We demonstrate the accumulated reward, accuracy and #steps along the training environment episodes in Figure 5. For all the 6 scenes, our algorithm achieves high accuracy and low #steps. The saturated reward curve indicates that our algorithm converges well. We observe  $s_3$  converges the fastest, hence we stop its training earlier than the others.  $r_0$  and  $s_4$  converge the slowest, this is mainly due to the fact that  $r_0$  has complex realistic scene layout and much smaller calibrated region (12.0%) compared to the other scenes (average: 27.38%), while  $s_4$  owns much larger scene area (103.0  $m^2$ ), which creates difficulties for policy learning compared to others (average: 37.38  $m^2$ ).

### E. More Details of the ACR-6 Dataset

To demonstrate more details about the ACR-6 dataset, we illustrate the pairwise comparison between the static and dynamic scenes for both look-down view and first-person view in Figure 6 and Figure 7 respectively. To create the dynamic variant of the static scene, we rearrange the furniture and manipulate the illumination in the environment.

### F. More Visual Results

We demonstrate more visual results for  $s_0$ ,  $s_1$ ,  $s_2$ ,  $s_3$ ,  $s_4$  and  $r_0$  in Figure 8, 9, 10, 11, 12 and 13 separately. For each scene, we visualize the learned long trajectory, emergence of turn-around behavior and comparison between navigation paths in static and dynamic scenes. We observe our algorithm consistently learns intelligent behavior for active localization in all the scenes.

Scene	s0	s1	s2	s3	s4	r0	Avg.
unlocalizable	(0.960, 23.1)	(0.877, 17.2)	(0.846, 13.7)	(0.905, 8.9)	(0.807, 21.5)	(0.896, 22.3)	(0.881, 17.7)
localizable	(0.972, 4.4)	(0.919, 7.0)	(0.905, 11.8)	(0.919, 8.4)	(0.950, 8.4)	(0.938, 10.3)	(0.933, 8.3)
entire	(0.966, 14.0)	(0.896, 12.3)	(0.876, 12.7)	(0.913, 8.6)	(0.870, 15.2)	(0.916, 16.4)	(0.906, 13.2)

Table 6: Evaluation of our algorithm on the localizable and unlocalizable region along with the entire scene. The metrics are formulated as (accuracy, #steps).

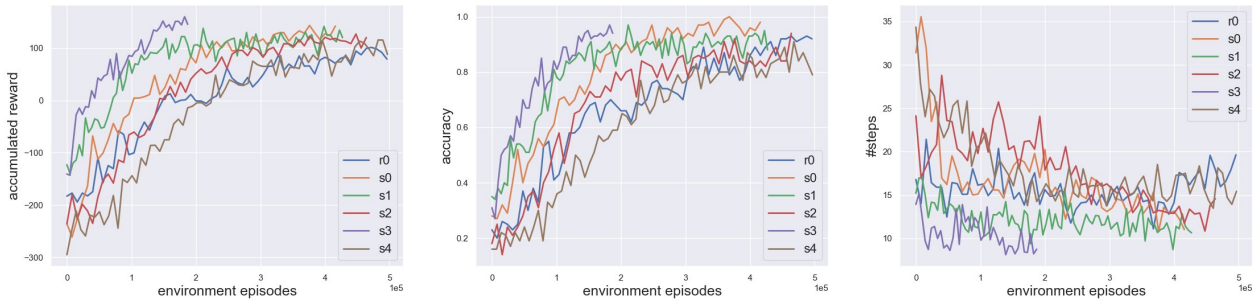


Figure 5: Training curves of the accumulated reward, accuracy and #steps for all the scenes in ACR-6 dataset.

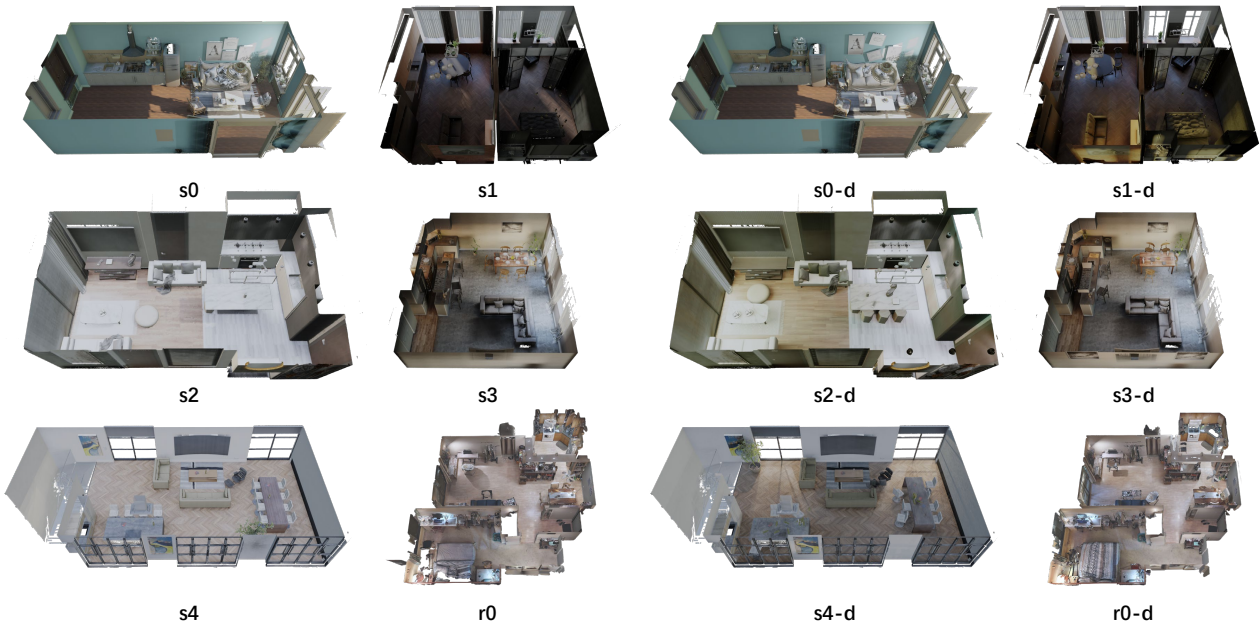


Figure 6: Comparison between the original static scene (left) and modified dynamic scene (right) from the look-down view. The geometry and illumination are changed to simulate the realistic dynamic environments. Zoom in to see the details.



Figure 7: Comparison between the static and dynamic scenes from the same first-person viewpoint in ACR-6 dataset.

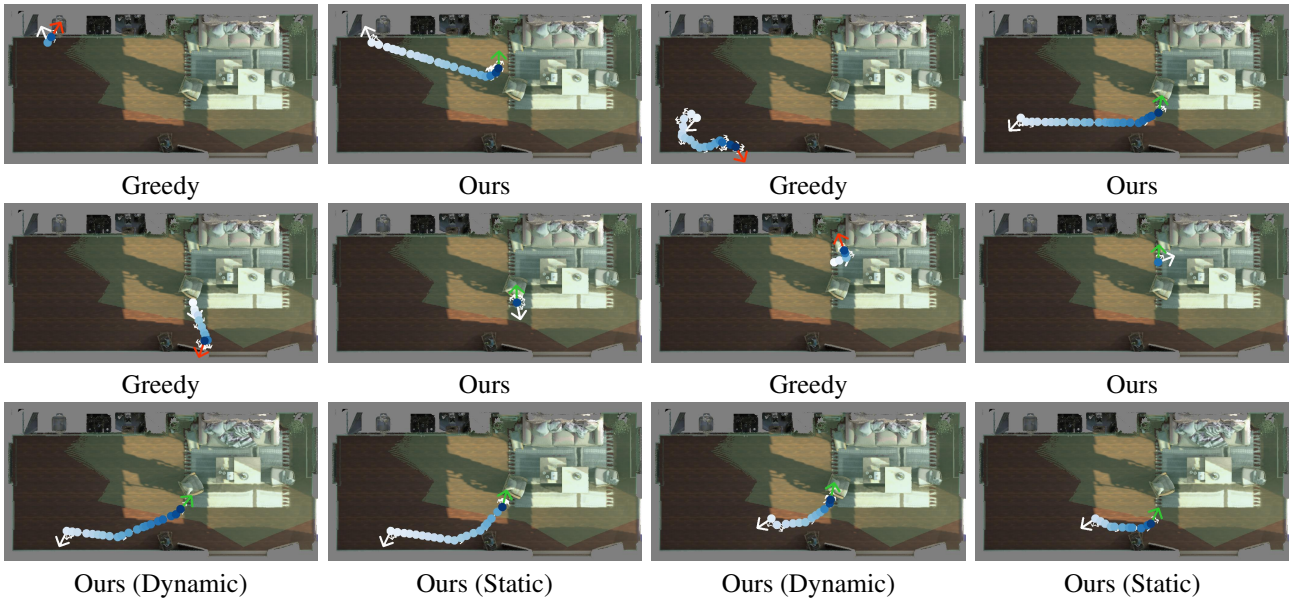


Figure 8: More visual results in  $s_0$ . First row: the agent travels along a long trajectory to localize itself; Second row: emergence of turn-around behavior; Third row: starting from roughly the same position, comparison between our learned navigation paths in static and dynamic scenes. The green and red arrow indicate the success and failure stop respectively. The shaded green area is the calibrated region.

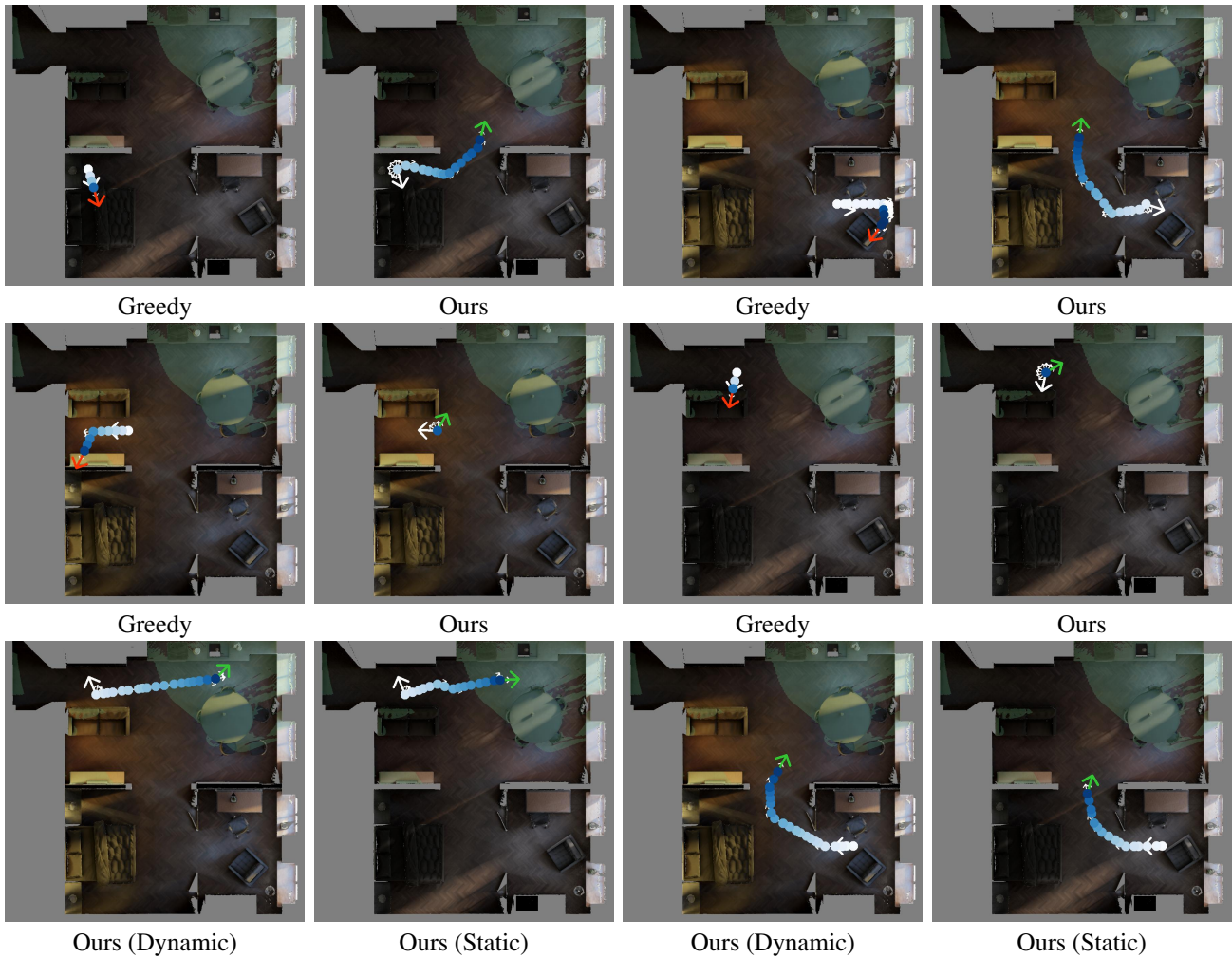


Figure 9: More visual results in  $s1$ . First row: the agent travels along a long trajectory to localize itself; Second row: emergence of turn-around behavior; Third row: starting from roughly the same position, comparison between our learned navigation paths in static and dynamic scenes. The green and red arrow indicate the success and failure stop respectively. The shaded green area is the calibrated region.

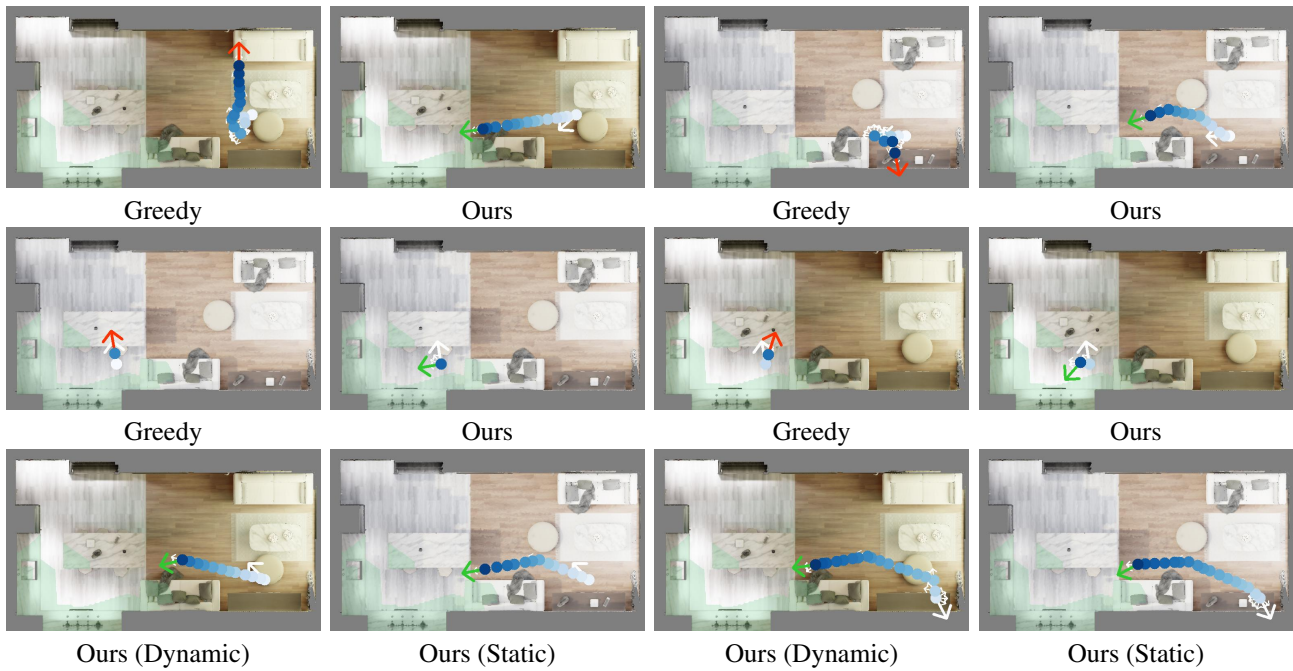


Figure 10: More visual results in  $s_2$ . First row: the agent travels along a long trajectory to localize itself; Second row: emergence of turn-around behavior; Third row: starting from roughly the same position, comparison between our learned navigation paths in static and dynamic scenes. The green and red arrow indicate the success and failure stop respectively. The shaded green area is the calibrated region.



Figure 11: More visual results in  $s_3$ . First row: the agent travels along a long trajectory to localize itself; Second row: emergence of turn-around behavior; Third row: starting from roughly the same position, comparison between our learned navigation paths in static and dynamic scenes. The green and red arrow indicate the success and failure stop respectively. The shaded green area is the calibrated region.

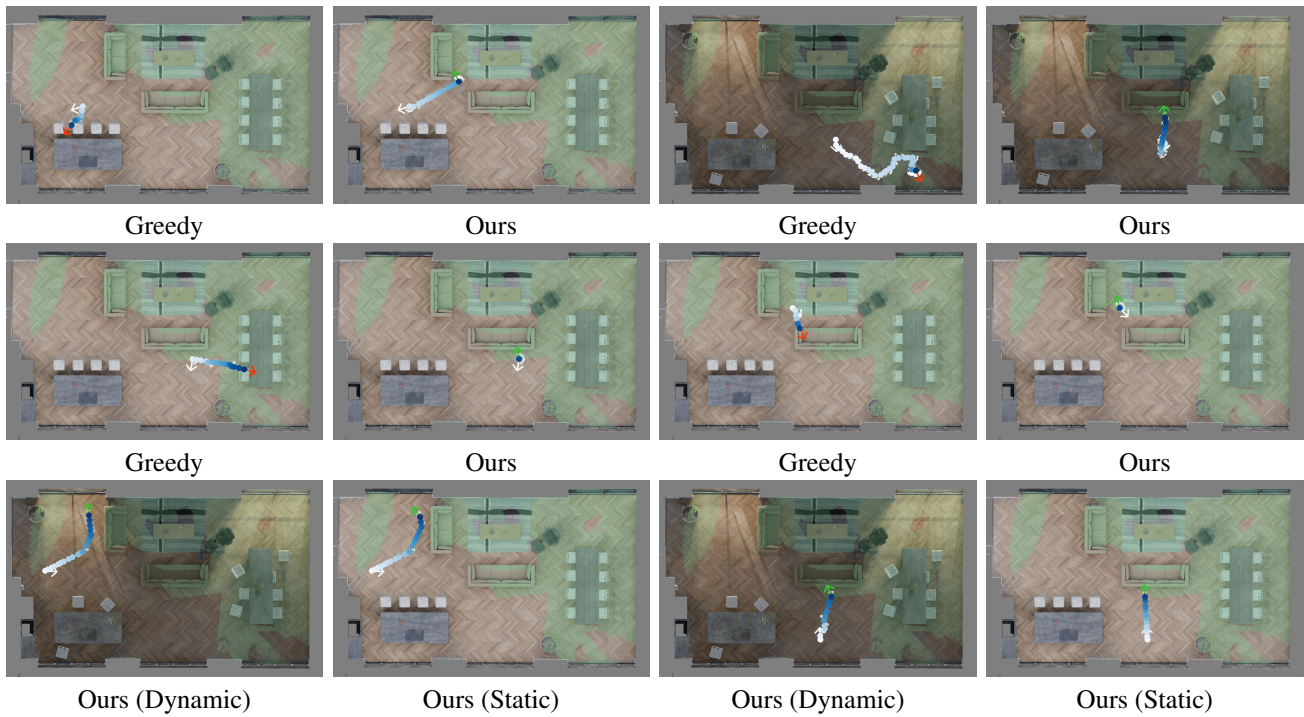


Figure 12: More visual results in  $s_4$ . First row: the agent travels along a long trajectory to localize itself; Second row: emergence of turn-around behavior; Third row: starting from roughly the same position, comparison between our learned navigation paths in static and dynamic scenes. The green and red arrow indicate the success and failure stop respectively. The shaded green area is the calibrated region.

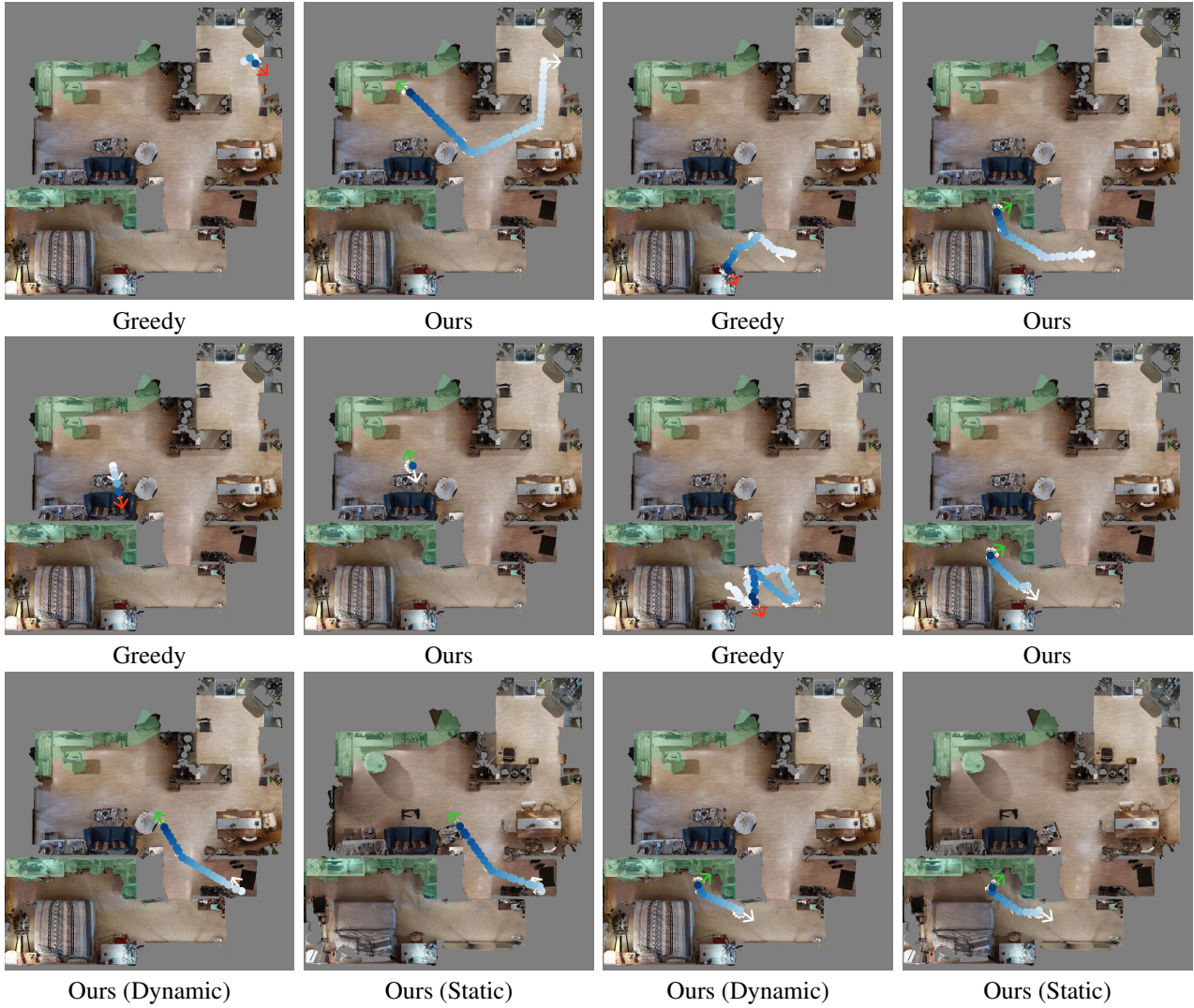


Figure 13: More visual results in  $r0$ . First row: the agent travels along a long trajectory to localize itself; Second row: emergence of turn-around behavior; Third row: starting from roughly the same position, comparison between our learned navigation paths in static and dynamic scenes. The green and red arrow indicate the success and failure stop respectively. The shaded green area is the calibrated region.

## References

- [1] Relja Arandjelovic, Petr Gronat, Akihiko Torii, Tomas Paszto, and Josef Sivic. Netvlad: Cnn architecture for weakly supervised place recognition. In *Proceedings of the IEEE conference on computer vision and pattern recognition*, pages 5297–5307, 2016. 2
- [2] Hernán Badino, D Huber, and Takeo Kanade. Visual topometric localization. In *2011 IEEE Intelligent Vehicles Symposium (IV)*, pages 794–799. IEEE, 2011. 3
- [3] Eric Brachmann, Alexander Krull, Sebastian Nowozin, Jamie Shotton, Frank Michel, Stefan Gumhold, and Carsten Rother. Dsac-differentiable ransac for camera localization. In *Proceedings of the IEEE Conference on Computer Vision and Pattern Recognition*, pages 6684–6692, 2017. 1, 2
- [4] Eric Brachmann, Frank Michel, Alexander Krull, Michael Ying Yang, Stefan Gumhold, et al. Uncertainty-driven 6d pose estimation of objects and scenes from a single rgb image. In *Proceedings of the IEEE conference on computer vision and pattern recognition*, pages 3364–3372, 2016. 2
- [5] Eric Brachmann and Carsten Rother. Learning less is more-6d camera localization via 3d surface regression. In *Proceedings of the IEEE Conference on Computer Vision and Pattern Recognition*, pages 4654–4662, 2018. 2, 8, 9
- [6] Eric Brachmann and Carsten Rother. Expert sample consensus applied to camera re-localization. In *Proceedings of the IEEE International Conference on Computer Vision*, pages 7525–7534, 2019. 2
- [7] Eric Brachmann and Carsten Rother. Neural-guided ransac: Learning where to sample model hypotheses. In *Proceedings of the IEEE International Conference on Computer Vision*, pages 4322–4331, 2019. 1, 2
- [8] Samarth Brahmabhatt, Jinwei Gu, Kihwan Kim, James Hays, and Jan Kautz. Geometry-aware learning of maps for camera localization. In *Proceedings of the IEEE Conference on Computer Vision and Pattern Recognition*, pages 2616–2625, 2018. 2
- [9] Tommaso Cavallari, Stuart Golodetz, Nicholas Lord, Julien Valentin, Victor Prisacariu, Luigi Di Stefano, and Philip HS Torr. Real-time rgb-d camera pose estimation in novel scenes using a relocalisation cascade. *IEEE transactions on pattern analysis and machine intelligence*, 2019. 1, 2
- [10] Tommaso Cavallari, Stuart Golodetz, Nicholas A Lord, Julien Valentin, Luigi Di Stefano, and Philip HS Torr. On-the-fly adaptation of regression forests for online camera relocalisation. In *Proceedings of the IEEE conference on computer vision and pattern recognition*, pages 4457–4466, 2017. 1, 2, 3, 4, 8, 9
- [11] Devendra Singh Chaplot, Emilio Parisotto, and Ruslan Salakhutdinov. Active neural localization. *arXiv preprint arXiv:1801.08214*, 2018. 1, 2, 6
- [12] Kevin Chen, Juan Pablo de Vicente, Gabriel Sepulveda, Fei Xia, Alvaro Soto, Marynel Vázquez, and Silvio Savarese. A behavioral approach to visual navigation with graph localization networks. *arXiv preprint arXiv:1903.00445*, 2019. 1, 2
- [13] Sean P Engelson and Drew V McDermott. Error correction in mobile robot map learning. In *Proceedings 1992 IEEE International Conference on Robotics and Automation*, pages 2555–2556. IEEE Computer Society, 1992. 1
- [14] Dieter Fox, Wolfram Burgard, and Sebastian Thrun. Active markov localization for mobile robots. *Robotics and Autonomous Systems*, 25(3):195–208, 1998. 1, 2
- [15] Saurabh Gupta, James Davidson, Sergey Levine, Rahul Sukthankar, and Jitendra Malik. Cognitive mapping and planning for visual navigation. In *Proceedings of the IEEE Conference on Computer Vision and Pattern Recognition*, pages 2616–2625, 2017. 1
- [16] Abner Guzman-Rivera, Pushmeet Kohli, Ben Glocker, Jamie Shotton, Toby Sharp, Andrew Fitzgibbon, and Shahram Izadi. Multi-output learning for camera relocalization. In *Proceedings of the IEEE conference on computer vision and pattern recognition*, pages 1114–1121, 2014. 2
- [17] Patric Jensfelt and Steen Kristensen. Active global localization for a mobile robot using multiple hypothesis tracking. *IEEE Transactions on Robotics and Automation*, 17(5):748–760, 2001. 1, 2
- [18] Leslie Pack Kaelbling, Michael L Littman, and Anthony R Cassandra. Planning and acting in partially observable stochastic domains. *Artificial intelligence*, 101(1-2):99–134, 1998. 2
- [19] Alex Kendall and Roberto Cipolla. Geometric loss functions for camera pose regression with deep learning. In *Proceedings of the IEEE Conference on Computer Vision and Pattern Recognition*, pages 5974–5983, 2017. 2
- [20] Alex Kendall, Matthew Grimes, and Roberto Cipolla. Posenet: A convolutional network for real-time 6-dof camera relocalization. In *Proceedings of the IEEE international conference on computer vision*, pages 2938–2946, 2015. 2
- [21] Diederik P Kingma and Jimmy Ba. Adam: A method for stochastic optimization. *arXiv preprint arXiv:1412.6980*, 2014. 6
- [22] Alexander Krull, Eric Brachmann, Sebastian Nowozin, Frank Michel, Jamie Shotton, and Carsten Rother. Poseagent: Budget-constrained 6d object pose estimation via reinforcement learning. In *Proceedings of the IEEE Conference on*

- Computer Vision and Pattern Recognition*, pages 6702–6710, 2017. 3
- [23] Jing Li, Chengyi Wang, Xuejie Kang, and Qiang Zhao. Camera localization for augmented reality and indoor positioning: A vision-based 3d feature database approach. *International Journal of Digital Earth*, 2019. 1
- [24] Xiaotian Li, Shuzhe Wang, Yi Zhao, Jakob Verbeek, and Juho Kannala. Hierarchical scene coordinate classification and regression for visual localization. 2020. 1, 2
- [25] Hyon Lim, Sudipta N Sinha, Michael F Cohen, and Matthew Uyttendaele. Real-time image-based 6-dof localization in large-scale environments. In *2012 IEEE conference on computer vision and pattern recognition*, pages 1043–1050. IEEE, 2012. 2
- [26] Cheng Lin, Tingxiang Fan, Wenping Wang, and Matthias Nießner. Modeling 3d shapes by reinforcement learning. *arXiv preprint arXiv:2003.12397*, 2020. 3
- [27] David G Lowe. Distinctive image features from scale-invariant keypoints. *International journal of computer vision*, 60(2):91–110, 2004. 2
- [28] Tiange Luo, Kaichun Mo, Zhiao Huang, Jiarui Xu, Siyu Hu, Liwei Wang, and Hao Su. Learning to group: A bottom-up framework for 3d part discovery in unseen categories. *arXiv preprint arXiv:2002.06478*, 2020. 3
- [29] Gian Luca Mariottini and Stergios I Roumeliotis. Active vision-based robot localization and navigation in a visual memory. In *2011 IEEE International Conference on Robotics and Automation*, pages 6192–6198. IEEE, 2011. 1, 2
- [30] Daniela Massiceti, Alexander Krull, Eric Brachmann, Carsten Rother, and Philip HS Torr. Random forests versus neural networks—what’s best for camera localization? In *2017 IEEE International Conference on Robotics and Automation (ICRA)*, pages 5118–5125. IEEE, 2017. 2
- [31] Stefan Mathe, Aleksis Pirinen, and Cristian Sminchisescu. Reinforcement learning for visual object detection. In *Proceedings of the IEEE Conference on Computer Vision and Pattern Recognition*, pages 2894–2902, 2016. 3
- [32] Lili Meng, Jianhui Chen, Frederick Tung, James J Little, Julien Valentin, and Clarence W de Silva. Backtracking regression forests for accurate camera relocalization. In *2017 IEEE/RSJ International Conference on Intelligent Robots and Systems (IROS)*, pages 6886–6893. IEEE, 2017. 2
- [33] Lili Meng, Frederick Tung, James J Little, Julien Valentin, and Clarence W de Silva. Exploiting points and lines in regression forests for rgb-d camera relocalization. In *2018 IEEE/RSJ International Conference on Intelligent Robots and Systems (IROS)*, pages 6827–6834. IEEE, 2018. 2
- [34] Charles Ruizhongtai Qi, Li Yi, Hao Su, and Leonidas J Guibas. Pointnet++: Deep hierarchical feature learning on point sets in a metric space. In *Advances in neural information processing systems*, pages 5099–5108, 2017. 5
- [35] Liangliang Ren, Xin Yuan, Jiwen Lu, Ming Yang, and Jie Zhou. Deep reinforcement learning with iterative shift for visual tracking. In *Proceedings of the European Conference on Computer Vision (ECCV)*, pages 684–700, 2018. 3
- [36] Paul-Edouard Sarlin, Cesar Cadena, Roland Siegwart, and Marcin Dymczyk. From coarse to fine: Robust hierarchical localization at large scale. In *Proceedings of the IEEE Conference on Computer Vision and Pattern Recognition*, pages 12716–12725, 2019. 2
- [37] Paul-Edouard Sarlin, Frédéric Debraine, Marcin Dymczyk, Roland Siegwart, and Cesar Cadena. Leveraging deep visual descriptors for hierarchical efficient localization. *arXiv preprint arXiv:1809.01019*, 2018. 2
- [38] Torsten Sattler, Michal Havlena, Konrad Schindler, and Marc Pollefeys. Large-scale location recognition and the geometric burstiness problem. In *Proceedings of the IEEE Conference on Computer Vision and Pattern Recognition*, pages 1582–1590, 2016. 2
- [39] Torsten Sattler, Bastian Leibe, and Leif Kobbelt. Fast image-based localization using direct 2d-to-3d matching. In *2011 International Conference on Computer Vision*, pages 667–674. IEEE, 2011. 2
- [40] Torsten Sattler, Bastian Leibe, and Leif Kobbelt. Efficient & effective prioritized matching for large-scale image-based localization. *IEEE transactions on pattern analysis and machine intelligence*, 39(9):1744–1756, 2016. 2
- [41] Torsten Sattler, Will Maddern, Carl Toft, Akihiko Torii, Lars Hammarstrand, Erik Stenborg, Daniel Safari, Masatoshi Okutomi, Marc Pollefeys, Josef Sivic, et al. Benchmarking 6dof outdoor visual localization in changing conditions. In *Proceedings of the IEEE Conference on Computer Vision and Pattern Recognition*, pages 8601–8610, 2018. 3
- [42] Torsten Sattler, Qunjie Zhou, Marc Pollefeys, and Laura Leal-Taixe. Understanding the limitations of cnn-based absolute camera pose regression. In *Proceedings of the IEEE Conference on Computer Vision and Pattern Recognition*, pages 3302–3312, 2019. 2
- [43] John Schulman, Filip Wolski, Prafulla Dhariwal, Alec Radford, and Oleg Klimov. Proximal policy optimization algorithms. *arXiv preprint arXiv:1707.06347*, 2017. 6
- [44] Jianzhun Shao, Yuhang Jiang, Gu Wang, Zhigang Li, and Xiangyang Ji. Pfrl: Pose-free reinforcement learning for 6d pose estimation. In *Proceedings of the IEEE/CVF Conference on Computer Vision and Pattern Recognition*, pages 11454–11463, 2020. 3
- [45] Jamie Shotton, Ben Glocker, Christopher Zach, Shahram Izadi, Antonio Criminisi, and Andrew Fitzgibbon. Scene coordinate regression forests for camera relocalization in rgb-d images. In *Proceedings of the IEEE Conference on Computer Vision and Pattern Recognition*, pages 2930–2937, 2013. 1, 2, 3, 6
- [46] Juil Sock, Guillermo Garcia-Hernando, and Tae-Kyun Kim. Active 6d multi-object pose estimation in cluttered scenarios with deep reinforcement learning. *IROS*, 2020. 3
- [47] James Supancic III and Deva Ramanan. Tracking as online decision-making: Learning a policy from streaming videos with reinforcement learning. In *Proceedings of the IEEE International Conference on Computer Vision*, pages 322–331, 2017. 3
- [48] Hajime Taira, Masatoshi Okutomi, Torsten Sattler, Mircea Cimpoi, Marc Pollefeys, Josef Sivic, Tomas Pajdla, and Akihiko Torii. Inloc: Indoor visual localization with dense matching and view synthesis. In *Proceedings of the IEEE Conference on Computer Vision and Pattern Recognition*, pages 7199–7209, 2018. 2, 3
- [49] Julien Valentin, Angela Dai, Matthias Nießner, Pushmeet Kohli, Philip Torr, Shahram Izadi, and Cem Keskin. Learning

- to navigate the energy landscape. In *2016 Fourth International Conference on 3D Vision (3DV)*, pages 323–332. IEEE, 2016. [3](#), [6](#)
- [50] Julien Valentin, Matthias Nießner, Jamie Shotton, Andrew Fitzgibbon, Shahram Izadi, and Philip HS Torr. Exploiting uncertainty in regression forests for accurate camera relocalization. In *Proceedings of the IEEE conference on computer vision and pattern recognition*, pages 4400–4408, 2015. [2](#)
- [51] Johanna Wald, Torsten Sattler, Stuart Golodetz, Tommaso Cavallari, and Federico Tombari. Beyond controlled environments: 3d camera re-localization in changing indoor scenes. *arXiv preprint arXiv:2008.02004*, 2020. [3](#), [6](#)
- [52] Bing Wang, Changhao Chen, Chris Xiaoxuan Lu, Peijun Zhao, Niki Trigoni, and Andrew Markham. Atloc: Attention guided camera localization. 2020. [2](#)
- [53] Fei Xia, William B Shen, Chengshu Li, Priya Kasimbeg, Micael Edmond Tchammi, Alexander Toshev, Roberto Martín-Martín, and Silvio Savarese. Interactive gibbon benchmark: A benchmark for interactive navigation in cluttered environments. *IEEE Robotics and Automation Letters*, 5(2):713–720, 2020. [6](#)
- [54] Qingyong Xie and Yongcai Wang. A survey of filtering based active localization methods. In *Proceedings of the 2020 the 4th International Conference on Big Data and Internet of Things*, pages 69–73, 2020. [2](#)
- [55] Luwei Yang, Ziqian Bai, Chengzhou Tang, Honghua Li, Yasutaka Furukawa, and Ping Tan. Sanet: Scene agnostic network for camera localization. In *Proceedings of the IEEE International Conference on Computer Vision*, pages 42–51, 2019. [2](#)
- [56] Yuke Zhu, Roozbeh Mottaghi, Eric Kolve, Joseph J Lim, Abhinav Gupta, Li Fei-Fei, and Ali Farhadi. Target-driven visual navigation in indoor scenes using deep reinforcement learning. In *2017 IEEE international conference on robotics and automation (ICRA)*, pages 3357–3364. IEEE, 2017. [1](#)